# Description and application of a 2D-axisymmetric model for entropy noise in nozzle flows

Ariane Emmanuelli, Jun Zheng, Maxime Huet, Alexis Giauque, Thomas Le Garrec, Sebastien Ducruix

# Description and application of a 2D-axisymmetric model for entropy noise in nozzle flows

Ariane Emmanuelli[a,*], Jun Zheng[a], Maxime Huet[a], Alexis Giauque[b], Thomas Le Garrec[a], Sébastien Ducruix[c]

[a] *DAAA, ONERA, Université Paris Saclay, F-92322 Châtillon, France*
[b] *LMFA - Laboratoire de Mécanique des Fluides et d'Acoustique, Ecole Centrale de Lyon, 36 avenue Guy de Collongue, 69134 Ecully Cedex, France*
[c] *Laboratoire EM2C, CNRS, CentraleSupélec, Université Paris-Saclay, 3, rue Joliot Curie, 91192 Gif-sur-Yvette cedex, France*

**Abstract**

Entropy noise corresponds to acoustic fluctuations generated inside gas-turbine engines when temperature (entropy) spots are accelerated by the mean flow. This type of noise currently faces growing interest because of its contribution to global aero-engine noise as well as its impact on combustion instabilities. In the present article, a two-dimensional semi-analytical model is developed to predict entropy noise in nozzle flow. It complements the reference model of Marble and Candel ("Acoustic disturbance from gas non-uniformities convected through a nozzle", J. Sound Vib., 55, pp. 225-243, 1977) and its more recent extensions which remain one-dimensional, by taking the radial variations of the flow into account in the noise generation computation. Validations are performed by comparison with computational aeroacoustics simulations with either entropy or acoustic excitations in a subsonic nozzle. Very good agreement is observed between the numerical simulations and the 2D model for all the frequencies considered. The role of entropy wave distortion in noise generation is demonstrated by comparison with a 1D model which fails to reproduce the simulated results for medium to large frequencies.

*Keywords:* entropy noise, nozzle, low-order modelling, computational aeroacoustics

## 1. Introduction

With the rapid increase of air traffic, noise disturbances around airports have become a critical issue. Solutions are needed to reduce the noise emitted by aircraft, a significant portion of which comes from the engine. Until recently, the predominant fan and jet noise in turbofans masked internal sources such

*Corresponding author
*Email address:* aemmanuelli@online.fr (Ariane Emmanuelli)

as combustion noise. However, it is becoming a major contributor as other sources are reduced, and it is even dominant at certain frequencies and operating points [1, 2] . With no fan and low jet speeds, combustion noise is also significant in turboshaft engines [3, 4] . In addition, the emitted acoustic waves affect the flame in the combustion chamber [5], and as such they can play a significant role in the development of thermo-acoustic instabilities, the improved prediction of which could lead to reduced $NO_x$ emissions.

Combustion noise is made of two distinct phenomena [6]. Direct noise is emitted within the combustion chamber itself and it originates from fluctuations in heat release of the flame. It was tackled first and has been studied more extensively [2]. On the other hand, indirect combustion noise is generated by the presence of heterogeneities produced by the combustion process, convected downstream and accelerated through the turbine stages and nozzles. There are three types of perturbations: compositional [7], vortical [8] and entropic [9]. The latter results in what is also called entropy noise, which sparks the most interest as it constitutes the largest contribution to indirect combustion noise [10]. The entropy noise generation mechanism is classically associated with mode coupling. As entropy perturbations are accelerated, they interact with acoustic and vortical modes, leading to the emission of acoustic and vorticity waves [11]. A more physical explanation for entropy noise is that acoustic waves are emitted to maintain pressure balance as entropy waves are expanded in accelerated flow [12].

The basis of entropy noise theory was established in the 1970s. A model for the compact nozzle, the length of which is negligible compared to wavelengths, was developed based on conservation principles, with an extension to non-compact nozzles of linear velocity profiles [13]. Similarly, a model for the compact turbine was derived [14]. Interest in indirect combustion noise was renewed in more recent years with the increase of its relative contribution to the noise emitted by engines as a whole. The research community aims at describing the full noise generation process including the production of heterogeneities in the combustion chamber [15], their attenuation [16], their acceleration through the nozzles [17] and turbine stages [18] leading to indirect combustion noise, and how these perturbations and acoustic waves exit the engine [19]. Investigation of entropy noise generation naturally focused on the simpler nozzle configurations first.

Experimental investigations of a laboratory combustor with a nozzle, which aimed at evaluating the direct and indirect contributions to combustion noise at different operating points, highlighted the difficulty to measure temperature fluctuations at the exit of the chamber [20]. The EWG (Entropy Wave Generator) experiment was set-up at DLR to focus on entropy noise. It overcame problems caused by the presence of a combustor by using hot wires to produce hot-spots. Entropy noise characterisation was improved and its significance confirmed, but the entropy noise generation mechanism remained difficult to apprehend [21]. This experiment constituted a first reference case for entropy noise, the results of which were confirmed by numerical studies [21–23] which led to better understanding of the acoustic reflections within the experimental

setup and improved modelling of the heat source used to produce hot pulses [24–26]. Large Eddy Simulation (LES) is classically chosen for these studies for its higher-fidelity predictions, especially for comparisons with experiment, but Computational AeroAcoustics (CAA) methods have also been used successfully, for example to underline the significant contribution of entropy noise to combustion noise [27], at much lower cost. Another test-facility at DLR allowed to further investigate the reasons for increased entropy noise, and in particular the role of temperature gradient, mass-flow rate and hot-spot three dimensionality, as well as the use of bias flow liners for noise reduction [28, 29]. An EWG experiment was also set-up at Cambridge in an effort to investigate both direct and indirect combustion noise and their relative contributions, as well as to obtain data for the validation of analytical work [30]. Long ducts and convective times led to clear separation of direct and indirect noise. Both orifice plates and nozzles were investigated using an electrical heating device like at DLR, as well as pulsed injection of helium to study both entropy and compositional noise [10]. For the first time, data was measured upstream of the source in this test-facility, making it complementary to other experimental data available for validations. In addition to laboratory experiments, data from real engines was collected in an effort to identify the contribution of entropy noise in more realistic conditions [31–33] by comparison with theoretical [34] or numerical work [35].

Even with such advances, extreme operating conditions, chemical reactions, separation of direct and indirect contributions, challenging temperature measurements, acoustic reflection and the duration of numerical simulations necessary to capture acoustic fluctuations are some reasons why entropy noise remains complex and costly to investigate numerically and experimentally. This motivates the development of analytical methods which constitute an interesting additional tool to better understand entropy noise, and which may become a cost-effective alternative for engineering developments. To this purpose, Marble and Candel's model [13] was adapted to get rid of its initial limitations. It was extended to the non-linear regime for compact nozzles [36] and in the linear regime to nozzles of arbitrary shape in 1D (non-compact assumption), for both subcritical and chocked nozzles [37–41]. More recently, the compact solution was used as part of a model for both direct and indirect combustion noise which was compared to experimental results [42] and which has been extended to non-isentropic nozzle flow [43]. The presence of circumferential waves has also been included [1, 44]. However, limitations remain and it seems radial variations need to be taken into account to increase the accuracy of estimated entropy noise levels.

Such transverse variations of the flow were first considered in studies focusing on the convection of entropy perturbations in channel flow [16, 45, 46]. They typically aim at evaluating entropy wave attenuation between the combustor and the turbine stages or nozzles where entropy noise is generated. Noise levels were found to be strongly affected by shear dispersion of the entropy perturbations, while dissipation proved negligible. Turbulent and thermal effects have also been investigated [46–48], as well as the impact of entropy dispersion at the turbine outlet of a real engine [49]. In addition, entropy dispersion has been modeled

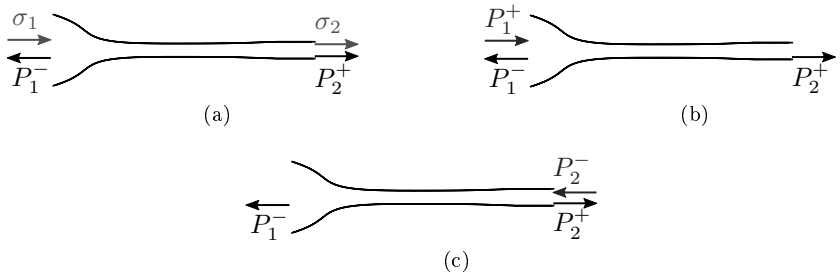


Figure 1: Diagrams of the waves present for each forcing type in the subsonic case. (a) entropic; (b) upstream acoustic; (c) downstream acoustic forcing.

in both nozzle and turbine geometries by computing an attenuation functions from mean flow variables [50–53]. These entropy convection models provide the attenuation of the entropy wave, which can then be taken into account as an input parameter to entropy noise models. However, its evaluation remains dissociated from entropy noise generation, for which compact or 1D models neglecting radial variations are used.

In this paper, a 2D-axisymmetric semi-analytical model is developed to provide a fast and accurate evaluation of entropy noise in nozzle flow. This model, named CHEOPS-Nozzle (*non-compact harmonic entropy noise predictions*), improves existing models by taking into account the radial variation of both the mean flow and entropy fluctuations directly in the noise generation process. The paper is organised as follows. The analytical developments and procedure for numerical resolution are provided in section 2. The accuracy of the model is evaluated in section 3, in which the noise generated and scattered through subsonic nozzle flow is compared to reference CAA data. The failure of the 1D models to recover numerical results is demonstrated. To end, conclusions and prospects are drawn in section 4.

## 2. Presentation of the 2D model

The 2D-axisymmetric semi-analytical model CHEOPS-Nozzle for entropy noise in nozzle flow is presented in this section. Figure 1 gives the different waves involved in the subsonic case. In diagram (a), normalised entropy fluctuations are noted $\sigma = s'/c_p$. As they are accelerated from position 1 at the inlet to the outlet noted 2, entropy noise is generated in the form of acoustic perturbations propagating upstream and downstream respectively, and which are noted $P_1^-$ and $P_2^+$ once normalised. The transfer functions $[P_1^-/\sigma_1]$ and $[P_2^+/\sigma_1]$ are used to describe these waves, generated by the acceleration of $\sigma_1$ through the domain. It can also be interesting to force the system acoustically to investigate the propagation and scattering of acoustic waves through the nozzle, in particular as noise sources other than entropy noise are present in engines. Figure 1 (b)

illustrates the case in which the wave $P_1^+$ is injected upstream and Fig. 1 (c) the configuration in which the flow is excited with $P_2^-$, propagating from the outlet of the domain. Both cases result in waves $P_1^-$ and $P_2^+$ propagating upstream and downstream respectively, as with entropic forcing. These waves can also be characterised using transfer functions: $[P_1^-/P_1^+]$ and $[P_2^+/P_1^+]$ in the case of upstream acoustic excitation, and $[P_1^-/P_2^-]$ and $[P_2^+/P_2^-]$ for forcing from downstream.

In a first instance, the objective of CHEOPS-Nozzle is to estimate the pressure and velocity fluctuations in order to compute these transfer functions for entropic, upstream acoustic or downstream acoustic forcing. This model is adapted from Zheng's work [54, 55] in curvilinear coordinates to cylindrical coordinates which are well suited to axisymmetric nozzle flow. The governing equations of the model are detailed in section 2.1 and the resolution process is given in section 2.2.

### *2.1. Fundamental assumptions and equations*

CHEOPS-Nozzle is based on the Euler equations and obeys the following assumptions:

1. all viscous terms are neglected, verifying the Euler equations,
2. pressure and velocity fluctuations are solely due to acoustics, thereby neglecting vorticity fluctuations,
3. the mean flow is considered 2D-axisymmetric, with variations in the axial and radial directions,
4. acoustic waves are considered one-dimensional throughout the domain, as radial modes are cut-off by the duct and azimuthal modes are neglected, assuming all fields are 2D-axisymmetric,
5. perturbations are small, allowing the linearisation of equations.

In order to estimate entropy noise, the entropy fluctuations $s'$ need to be computed throughout the domain, as well as the pressure and velocity fluctuations $p'$ and $u'$ which characterise the resulting one-dimensional acoustic waves. As entropy is purely convected, it can be computed numerically from mean flow quantities following a procedure described in the next section. This leaves two unknowns, so that two equations are needed. Mass conservation and momentum in the axial direction are chosen, as it is the main direction of the flow and the direction of acoustic wave propagation.

In its integral form, the continuity equation can be written:

$$\frac{\partial}{\partial t}\int_V \rho \mathrm{d}V = \int_A [\rho u_x](x)\mathrm{d}A - \int_A [\rho u_x](x+\mathrm{d}x)\mathrm{d}A \tag{1}$$

The radially dependent flow variables are reduced to one-dimensional quantities by averaging over each section of area A using the formula:

$$\overline{z} = \frac{1}{A}\int_A z \mathrm{d}A \tag{2}$$

and after some simplifications, Eq. (1) reduces to:

$$\frac{\partial \overline{\rho}}{\partial t} + \frac{\partial \overline{\rho u_x}}{\partial x} = -\frac{1}{A}\overline{\rho u_x}\frac{\mathrm{d}A}{\mathrm{d}x} \tag{3}$$

Sectional averaging is also applied to the axial-momentum equation, which writes:

$$\overline{\frac{\partial u_x}{\partial t}} + \overline{u_x \frac{\partial u_x}{\partial x}} + \overline{u_r \frac{\partial u_x}{\partial r}} = -\overline{\frac{1}{\rho}\frac{\partial p}{\partial x}} \tag{4}$$

Both these equations are linearised using flow variable decomposition into mean and perturbed quantities, such as $f = f_0 + f'$. Because of the one-dimensional acoustics assumption, the radial velocity fluctuation $u'_r = 0$ m/s and sectional averaging of acoustic fluctuations amounts to $\overline{u'}_x = u'_x$ and $\overline{p'} = p'$. In addition, the equations are given in terms of entropy and pressure fluctuations, $s'$ and $p'$, rather than density perturbations which can be expressed as $\rho' = p'/c_0^2 - \rho_0 s'/c_p$, with $c_0$ the velocity of sound and $c_p$ the heat capacity at constant pressure. The continuity and momentum equations in the direction of the flow then write:

$$\begin{aligned} A\left(\overline{\frac{1}{c_0^2}}\right)\frac{\partial p'}{\partial t} + \frac{\mathrm{d}}{\mathrm{d}x}\left[A\left(\overline{\frac{u_{0x}}{c_0^2}}\right)\right]p' + \left[A\left(\overline{\frac{u_{0x}}{c_0^2}}\right)\right]\frac{\partial p'}{\partial x} + \frac{\mathrm{d}A\overline{\rho}_0}{\mathrm{d}x}u'_x + A\overline{\rho}_0\frac{\partial u'_x}{\partial x} \\ = \frac{\partial}{\partial x}\left[A\overline{(\rho_0 u_{0x})\,\frac{s'}{c_p}}\right] + A\frac{\partial}{\partial t}\left(\overline{\rho_0\frac{s'}{c_p}}\right) \end{aligned} \tag{5}$$

$$\begin{aligned} \frac{\partial u'_x}{\partial t} + u'_x\left(\overline{\frac{\partial u_{0x}}{\partial x}}\right) + \overline{u}_{0x}\frac{\partial u'_x}{\partial x} + \left(\overline{\frac{1}{\rho_0}}\right)\frac{\partial p'}{\partial x} + \left[\overline{\frac{u_{0x}}{\gamma p_0}\frac{\partial u_{x0}}{\partial x}} + \overline{\frac{u_{0r}}{\gamma p_0}\frac{\partial u_{x0}}{\partial r}}\right]p' \\ = \overline{\left[u_{0x}\frac{\partial u_{x0}}{\partial x} + u_{0r}\frac{\partial u_{x0}}{\partial r}\right]\frac{s'}{c_p}} \end{aligned} \tag{6}$$

Note radial variations of the flow appear on the right hand side and in the last term on the left hand side of Eq. 6, affecting the entropy noise source term and acoustic scattering respectively. Next, the harmonic regime is considered in order to eliminate terms involving temporal derivatives. Under this condition, fluctuations can be written in the form:

$$u'_x(x,t) = \hat{u}(x)\mathrm{e}^{\mathrm{i}\omega t} \tag{7}$$

$$p'(x,t) = \hat{p}(x)\mathrm{e}^{\mathrm{i}\omega t} \tag{8}$$

$$\frac{s'}{c_p}(x,t) = \hat{\sigma}(x)\mathrm{e}^{\mathrm{i}\omega t} \tag{9}$$

where $\hat{u}, \hat{p}$ and $\hat{\sigma}$ are the complex amplitudes of the velocity, pressure and normalised entropy fluctuations. The angular frequency is noted $\omega = 2\pi f$, with $f$ the frequency. The mass conservation and momentum equations, Eqs. (5)-(6), can ultimately be written:

$$\begin{aligned} \left(A\left(\overline{\frac{1}{c_0^2}}\right)\mathrm{i}\omega + \frac{\mathrm{d}}{\mathrm{d}x}\left[A\left(\overline{\frac{u_{0x}}{c_0^2}}\right)\right]\right)\hat{p} + \left[A\left(\overline{\frac{u_{0x}}{c_0^2}}\right)\right]\frac{\partial \hat{p}}{\partial x} + \frac{\mathrm{d}A\overline{\rho}_0}{\mathrm{d}x}\hat{u} + A\overline{\rho}_0\frac{\partial \hat{u}}{\partial x} \\ = \frac{\mathrm{d}}{\mathrm{d}x}\left[A\overline{(\rho_0 u_{0x})\,\hat{\sigma}}\right] + A\mathrm{i}\omega\overline{\rho_0\hat{\sigma}} \end{aligned} \tag{10}$$

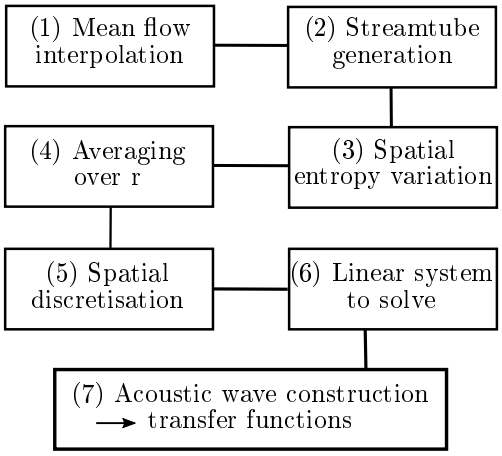


Figure 2: Resolution process of CHEOPS-Nozzle.

$$\left[\overline{\frac{u_{0x}}{\gamma p_0}\frac{\partial u_{x0}}{\partial x}} + \overline{\frac{u_{0r}}{\gamma p_0}\frac{\partial u_{x0}}{\partial r}}\right]\hat{p} + \left(\overline{\frac{1}{\rho_0}}\right)\frac{\partial p'}{\partial x} + \left[\mathrm{i}\omega + \left(\overline{\frac{\partial u_{0x}}{\partial x}}\right)\right]\hat{u} + \overline{u}_{0x}\frac{\partial \hat{u}}{\partial x} = \overline{\left[u_{0x}\frac{\partial u_{x0}}{\partial x} + u_{0r}\frac{\partial u_{x0}}{\partial r}\right]}\hat{\sigma} \tag{11}$$

Equations (10)-(11) form a system of two equations and two unknowns $\hat{u}$ and $\hat{p}$. Its numerical resolution is detailed in the next paragraph.

### *2.2. Numerical implementation*

The resolution process of CHEOPS-Nozzle is made of the steps given in Fig. 2 and described in this section. In steps 1-3, the input variables of Eqs. (10)-(11) are processed. Steps 4-6 then enable the system of equations to be solved numerically, before post-processing step 7.

*Step 1.* The model uses two-dimensional mean flow fields as an input. They can be obtained by any method, typically Computational Fluid Dynamics (CFD): Euler simulation, RANS, or even LES for instance. These fields must be interpolated by the user onto a 2D-axisymmetric structured mesh. Note the use of one-dimensional mean flow resulted in the same transfer functions as those predicted by a one-dimensional model.

*Step 2.* In order to compute entropy variations in the following step, the mean flow fields are radially divided into streamtubes by the model using a time marching method. In the case of turbine flow, streamlines were also used by Leyko et al. [52] to take transverse mean flow variations into account. They computed the delay compared to 1D flow at a point downstream of the blade row, in order to estimate the resulting attenuation of entropy perturbations. In the present study, the model for entropy noise uses mean flow variables throughout

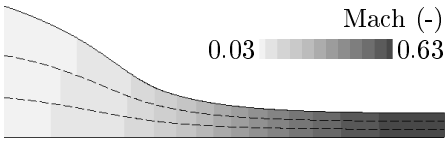


Figure 3: Contour of the Mach number averaged by the model in three streamtubes delimited by streamlines (dashed lines) in the convergent section of the nozzle.

the blade passage directly. They are sectionally averaged in each streamtube, which is illustrated for 3 streamtubes in Fig. 3.

*Step 3.* As entropy is a quantity convected by the mean flow without attenuation or distortion in subsonic flow governed by the Euler equations, the entropy fluctuations are then transported numerically using the mean velocity by integration along each streamtube:

$$\frac{s'}{c_p}(l,t) = \frac{s'}{c_p}\left(l = 0, t - \int_0^l \frac{\mathrm{d}\zeta}{\|u(\zeta)\|}\right) \tag{12}$$

A sufficient number of streamtubes is required to accurately capture the radial variation of the entropy perturbations. The mesh must also be discretised enough in the axial direction to prevent entropy wave dispersion errors. Different phases can be chosen in each streamtube, so that any radial distribution of the entropy fluctuations can be set at the inlet. In this paper, only planar entropy waves are considered.

*Step 4.* With both mean flow variables and entropy fluctuations obtained in two dimensions to take radial variations into account, they can be sectionally averaged as described in section 2.1, as acoustic waves are assumed one-dimensional. The system made of Eqs. (10)-(11) can then be solved.

*Step 5.* To this end, second order spatial discretisation is applied in the axial direction. The equations are evaluated at the centre of each element noted $c_k$, while the unknowns, that is the perturbed flow variables $\hat{p}$ and $\hat{u}$, are sought at nodes $k$. Then, using the relations:

$$f_{c_k} = \frac{f_{k+1} + f_k}{2} \tag{13}$$

$$\frac{\partial}{\partial x} f_{c_k} = \frac{f_{k+1} - f_k}{\Delta x_{c_k}} \tag{14}$$

where $\Delta x_{c_k}$ is the size of element $c_k$ in the axial direction, the continuity and momentum equations (10)-(11) become:

$$\lambda^1_{c_k}\hat{p}_k + \lambda^2_{c_k}\hat{u}_k + \lambda^3_{c_k}\hat{p}_{k+1} + \lambda^4_{c_k}\hat{u}_{k+1} = \hat{S}^C_{c_k} \tag{15}$$

$$\phi^1_{c_k}\hat{p}_k + \phi^2_{c_k}\hat{u}_k + \phi^3_{c_k}\hat{p}_{k+1} + \phi^4_{c_k}\hat{u}_{k+1} = \hat{S}^M_{c_k} \tag{16}$$

where $\hat{p}_k$ and $\hat{u}_k$ are the pressure and velocity fluctuation amplitudes evaluated at node $k$, $\lambda^j_{c_k}$ and $\phi^j_{c_k}$ are cell-centered coefficients at element $c_k$ which depend on the mean flow variables, and the source terms $\hat{S}^C_{c_k}$ and $\hat{S}^M_{c_k}$ are also evaluated at the center of $c_k$. These coefficients can be expressed as:

$$\lambda^1_{c_k} = \left(\frac{1}{2}\left[A\overline{\left(\frac{1}{c_0^2}\right)}\mathrm{i}\omega + \frac{\mathrm{d}}{\mathrm{d}x}\left[A\overline{\left(\frac{u_{0x}}{c_0^2}\right)}\right]\right] - \frac{A}{\Delta x}\overline{\left(\frac{u_{0x}}{c_0^2}\right)}\right)_{c_k} \tag{17}$$

$$\lambda^2_{c_k} = \left(\frac{1}{2}\frac{\mathrm{d}A\overline{\rho}_0}{\mathrm{d}x} - \frac{A\overline{\rho}_0}{\Delta x}\right)_{c_k} \tag{18}$$

$$\lambda^3_{c_k} = \left(\frac{1}{2}\left[A\overline{\left(\frac{1}{c_0^2}\right)}\mathrm{i}\omega + \frac{\mathrm{d}}{\mathrm{d}x}\left[A\overline{\left(\frac{u_{0x}}{c_0^2}\right)}\right]\right] + \frac{A}{\Delta x}\overline{\left(\frac{u_{0x}}{c_0^2}\right)}\right)_{c_k} \tag{19}$$

$$\lambda^4_{c_k} = \left(\frac{1}{2}\frac{\mathrm{d}A\overline{\rho}_0}{\mathrm{d}x} + \frac{A\overline{\rho}_0}{\Delta x}\right)_{c_k} \tag{20}$$

$$\phi^1_{c_k} = \left(\frac{1}{2}\left[\overline{\left(\frac{u_{0x}}{\gamma p_0}\frac{\partial u_{0x}}{\partial x}\right)} + \overline{\left(\frac{u_{0r}}{\gamma p_0}\frac{\partial u_{0x}}{\partial r}\right)}\right] - \frac{1}{\Delta x}\overline{\left(\frac{1}{\rho_0}\right)}\right)_{c_k} \tag{21}$$

$$\phi^2_{c_k} = \left(\frac{1}{2}\left[\mathrm{i}\omega + \overline{\left(\frac{\partial u_{0x}}{\partial x}\right)}\right] - \frac{1}{\Delta x}\overline{u}_{0x}\right)_{c_k} \tag{22}$$

$$\phi^3_{c_k} = \left(\frac{1}{2}\left[\overline{\left(\frac{u_{0x}}{\gamma p_0}\frac{\partial u_{0x}}{\partial x}\right)} + \overline{\left(\frac{u_{0r}}{\gamma p_0}\frac{\partial u_{0x}}{\partial r}\right)}\right] + \frac{1}{\Delta x}\overline{\left(\frac{1}{\rho_0}\right)}\right)_{c_k} \tag{23}$$

$$\phi^4_{c_k} = \left(\frac{1}{2}\left[\mathrm{i}\omega + \overline{\left(\frac{\partial u_{0x}}{\partial x}\right)}\right] + \frac{1}{\Delta x}\overline{u}_{0x}\right)_{c_k} \tag{24}$$

$$\hat{S}^C_{c_k} = \left(\frac{\mathrm{d}}{\mathrm{d}x}\left[A\overline{(\rho_0 u_{0x}\hat{\sigma})}\right] + A\mathrm{i}\omega\overline{(\rho_0\hat{\sigma})}\right)_{c_k} \tag{25}$$

$$\hat{S}^M_{c_k} = \left(\overline{\left[\left(u_{0x}\frac{\partial u_{0x}}{\partial x}\right) + \left(u_{0r}\frac{\partial u_{0x}}{\partial r}\right)\right]\hat{\sigma}}\right)_{c_k} \tag{26}$$

Notice the acoustic source terms $\hat{S}^C_{c_k}$ and $\hat{S}^M_{c_k}$ given by Eqs. (25)-(26) cancel out in the case of uniform flow.

*Step 6.* Boundary conditions are required to close the system of Eqs. (15)-(16). Physically, they are the acoustic waves entering the domain from the inlet and the outlet. The relations between the pressure and velocity fluctuations $\hat{p}$ and $\hat{u}$ and the normalised upstream and downstream propagating components of acoustic waves $P^-$ and $P^+$ are given by the Riemann invariants, under the condition $\hat{p}$ and $\hat{u}$ are purely acoustical which is one of the model's assumptions. They write:

$$P^{\pm} = \frac{1}{2}\left(\frac{\hat{p}}{\gamma\overline{p}_0} \pm \frac{\overline{\rho_0 c_0}}{\gamma\overline{p}_0}\hat{u}\right) \tag{27}$$

The choice of non-reflective boundaries is made, so that the acoustic waves entering the domain from the inlet and the outlet are imposed by the user directly. It also follows they can be written as a function of $\hat{p}$ and $\hat{u}$ using Eq. (27):

$$P_1^+ = \frac{1}{2}\left(\frac{\hat{p}}{\gamma\overline{p}_0} + \frac{\overline{\rho_0 c_0}}{\gamma\overline{p}_0}\hat{u}\right)_1 \tag{28}$$

$$P_n^- = \frac{1}{2}\left(\frac{\hat{p}}{\gamma\overline{p}_0} - \frac{\overline{\rho_0 c_0}}{\gamma\overline{p}_0}\hat{u}\right)_n \tag{29}$$

These two relations combined with Eqs. (15)-(16) result in a linear system of $2n$ equations with $2n$ unknowns which can be solved numerically for the pressure and velocity fluctuations $\hat{p}$ and $\hat{u}$. It is finally recast in matrix form:

$$\begin{pmatrix}
\left(\frac{1}{2\gamma\overline{p}_0}\right)_1 & \left(\frac{\overline{\rho_0 c_0}}{2\gamma\overline{p}_0}\right)_1 & 0 & .. & .. & .. & .. & .. & .. & .. \\
\lambda^1_{c_1} & \lambda^2_{c_1} & \lambda^3_{c_1} & \lambda^4_{c_1} & 0 & .. & .. & .. & .. & .. \\
\phi^1_{c_1} & \phi^2_{c_1} & \phi^3_{c_1} & \phi^4_{c_1} & 0 & .. & .. & .. & .. & .. \\
.. & .. & .. & .. & .. & .. & .. & .. & .. & .. \\
.. & .. & 0 & \lambda^1_{c_k} & \lambda^2_{c_k} & \lambda^3_{c_k} & \lambda^4_{c_k} & 0 & .. & .. \\
.. & .. & 0 & \phi^1_{c_k} & \phi^2_{c_k} & \phi^3_{c_k} & \phi^4_{c_k} & 0 & .. & .. \\
.. & .. & .. & .. & .. & .. & .. & .. & .. & .. \\
.. & .. & .. & .. & .. & 0 & \lambda^1_{c_{n-1}} & \lambda^2_{c_{n-1}} & \lambda^3_{c_{n-1}} & \lambda^4_{c_{n-1}} \\
.. & .. & .. & .. & .. & 0 & \phi^1_{c_{n-1}} & \phi^2_{c_{n-1}} & \phi^3_{c_{n-1}} & \phi^4_{c_{n-1}} \\
.. & .. & .. & .. & .. & .. & .. & 0 & \left(\frac{1}{2\gamma\overline{p}_0}\right)_n & -\left(\frac{\overline{\rho_0 c_0}}{2\gamma\overline{p}_0}\right)_n
\end{pmatrix}
\begin{pmatrix}
\hat{p}_1 \\ \hat{u}_1 \\ .. \\ \hat{p}_k \\ \hat{u}_k \\ \hat{p}_{k+1} \\ \hat{u}_{k+1} \\ .. \\ \hat{p}_n \\ \hat{u}_n
\end{pmatrix}
=
\begin{pmatrix}
P_1^+ \\ \hat{S}^C_{c_1} \\ \hat{S}^M_{c_1} \\ .. \\ \hat{S}^C_{c_k} \\ \hat{S}^M_{c_k} \\ .. \\ \hat{S}^C_{c_{n-1}} \\ \hat{S}^M_{c_{n-1}} \\ P_n^-
\end{pmatrix} \tag{30}$$

*Step 7.* The resulting fluctuations constitute acoustic perturbations which are separated into upstream and downstream propagating contributions, and which, again using the Riemann invariants defined in Eq. (27), are expressed:

$$P_1^- = \frac{1}{2}\left(\frac{\hat{p}}{\gamma\overline{p}_0} - \frac{\overline{\rho_0 c_0}}{\gamma\overline{p}_0}\hat{u}\right) \tag{31}$$

$$P_2^+ = \frac{1}{2}\left(\frac{\hat{p}}{\gamma\overline{p}_0} + \frac{\overline{\rho_0 c_0}}{\gamma\overline{p}_0}\hat{u}\right) \tag{32}$$

In this normalised form, noise levels can readily be presented in the form of transfer functions as described in the introduction of this section.

## 3. Numerical validation

Following the description of the model in general terms in the previous section, CHEOPS-Nozzle is applied in the next paragraphs and its results are verified and analysed using CAA. The DISCERN nozzle was chosen for this study. It was designed to investigate entropy noise within the European-FP7 project RECORD. A former version of this nozzle [56] was studied experimentally at

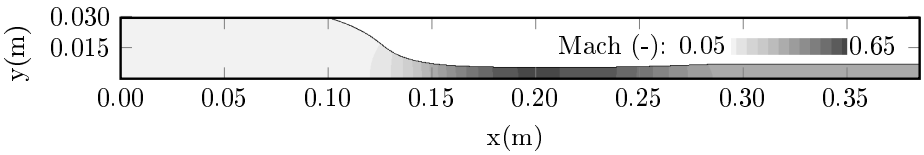


Figure 4: Contour of the Mach number in the DISCERN nozzle.

CentraleSupélec [20]. Unfortunately it could not be used to investigate entropy noise numerically because of massive flow separation. To avoid this, the geometry was adapted to the version used in this study, for which no experimental data is available. It is an axisymmetric nozzle, represented in Fig. 4.

The CAA approach allows to build a reference case in a framework similar to the model. Indeed, the linearised Euler equations are applied in both cases, while two of the model's main assumptions are relaxed by CAA:

- the acoustic waves are not assumed to be one-dimensional,
- vorticity is not neglected.

After a brief description of the application of CHEOPS-Nozzle to the DISCERN geometry, CAA methods are presented and analytical and numerical results are discussed in this section.

### *3.1. Application of the 2D model*

Mean flow fields obtained using any method can be used as an input to the model as described in section 2.2. In this case, the three-dimensional Euler equations are solved using the ONERA CFD code CEDRE with constant heat capacity ratio, in agreement with the model's assumptions. Conditions are based on those at the exit of a combustion chamber ($\gamma = 1.315$, $T_{inlet} = 1300$ K, $u_{x,inlet} = 12.53$ m/s) and on atmospheric conditions at the outlet of the domain ($P_{outlet} = 101325$Pa). Spatial discretisation is of second order in space and a pseudo-transient first order scheme is used in time. Figure 4 shows the Mach number throughout the 2D-axisymmetric domain. For this subsonic operating point, the Mach number reaches a maximum of 0.66 at the throat, it is quite low upstream at 0.02 and equal to 0.34 downstream. Convergence is verified and the relative mass flow rate error is smaller than $8.10^{-5}\%$.

These mean flow fields are interpolated onto a structured mesh, as described in the first step of the model's resolution process. The correct discretisation of the flow is verified by varying both the mesh size and the number of streamtubes, which also affects radial discretisation. Good convergence of the transfer functions was found with a $750,000$ element mesh and 50 streamtubes.

These parameters are used for 3 cases: one with entropic forcing to estimate entropy noise levels, and two with upstream and downstream acoustic forcing respectively to demonstrate the accurate propagation and scattering of acoustic waves more rigorously. In each case, plane waves are injected which corresponds

to setting the same entropy wave phase in all the streamtubes which form the computational domain. Transfer functions are then computed for frequencies between 0 and 1000 Hz with a step of 10 Hz.

### *3.2. CAA methods*

Like the model, CAA requires mean flow fields as an input. The same 2D-axisymmetric mean flow fields are used, after interpolation onto a 3D-structured CAA grid, in order to reduce the possibility of error when comparing analytical and numerical results. The computation then allows convection of flow perturbations such as the injected entropy wave, as well as acoustic generation and propagation. This section aims at presenting CAA numerical parameters and post-processing leading to the computation of transfer functions.

#### *3.2.1.* Numerical set-up

The ONERA code sAbrinA_v0 [57, 58] is used for entropy wave convection and acoustic propagation, as well as generation and convection of vorticity. The Euler equations are solved in their linear form, which corresponds to the model's assumptions. The simulations are made in the time domain, and the conservative variables are separated into mean and fluctuating contributions. Sixth order finite difference is used for spatial discretisation with tenth order explicit filtering, in order to avoid numerical dispersion and dissipation and to accurately capture acoustics. A third order explicit compact Runge-Kutta scheme is used in time. Boundary conditions derived by Tam et al. [59, 60] from the asymptotic solutions of the linearised Euler equations are used both to limit reflection at the boundaries of the domain and to inject entropic or acoustic plane waves. The 3D-structured mesh is made of five domains and a total of $2,500,000$ nodes. It is designed to have at least 16 points per acoustic or entropic wavelength at the highest frequency considered. The time-step is set to $8.10^{-8}$ seconds so the CFL number reaches a maximum at 0.73. Multi-harmonic simulations are used to limit numerical cost, with frequencies ranging from 100 to 1000 Hz with a step of 100 Hz. Two harmonic simulations with entropy forcing are also used both to validate the numerical methodology and to facilitate analysis of the results.

Verifications are made using entropic forcing. Mesh convergence is verified, as well as the agreement between the transfer-functions obtained using the harmonic and multi-harmonic CAA simulations. In addition, entropy conservation through the domain is verified using the ratio $\sigma_2/\sigma_1$. It is just under 0.98 on average, corresponding to a maximum numerical dissipation of the entropy waves of 2%, which is assumed negligible.

As with the model, the three cases of entropic, upstream acoustic and downstream acoustic excitation are simulated using CAA. Considering all three forcing types also allows to cancel out spurious acoustic reflections on domain boundaries using non-reflective post-processing, as described in the following section.

*3.2.2.* Post-processing

In order to analyse upstream and downstream propagating acoustic contributions, wave separation must first be applied to the fluctuations resulting from CAA. With CHEOPS-Nozzle, the Riemann invariants are used but this requires pressure and velocity fluctuations to be purely acoustical. This condition is not met downstream of the nozzle using CAA in the presence of entropy variations. Their acceleration generates vorticity [44] which affects velocity fluctuations, while it is neglected by the model. A direct mode matching method involving the purely acoustic pressure fluctuations only is therefore chosen. It is described by the following equations in the harmonic regime:

$$p' = p'^{+} + p'^{-} \tag{33}$$

$$\frac{\partial p'}{\partial x} = -\mathrm{i}k_x^{+} p'^{+} - \mathrm{i}k_x^{-} p'^{-} \tag{34}$$

where $p'^{-}$ and $p'^{+}$ are the pressure fluctuations propagating upstream and downstream respectively, and the wavenumbers are expressed as:

$$k_x^{+} = \frac{\omega}{u_0 + c_0},\ k_x^{-} = \frac{\omega}{u_0 - c_0} \tag{35}$$

The derivatives are evaluated using a finite difference scheme and the linear system can be solved for $p'^{+}$ and $p'^{-}$. This is achieved over several planes to reduce numerical error. In addition, it was verified both the Riemann invariants and the direct mode matching method lead to the same results upstream, where both pressure and velocity fluctuations are acoustical.

Wave reflection arising from numerical errors which may persist can be cancelled out by using results given by the three simulations, with entropic, upstream acoustic and downstream acoustic forcing respectively. To do so, the following system of six equations and six unknowns is solved to obtain the non-reflective transfer functions:

$$P_1{}^-(\sigma_1) = \left[\frac{P_1{}^-}{\sigma_1}\right]_{\mathrm{nr}} \sigma_1(\sigma_1) + \left[\frac{P_1{}^-}{P_1{}^+}\right]_{\mathrm{nr}} P_1{}^+(\sigma_1) + \left[\frac{P_1{}^-}{P_2{}^-}\right]_{\mathrm{nr}} P_2{}^-(\sigma_1) \tag{36}$$

$$P_2{}^+(\sigma_1) = \left[\frac{P_2{}^+}{\sigma_1}\right]_{\mathrm{nr}} \sigma_1(\sigma_1) + \left[\frac{P_2{}^+}{P_1{}^+}\right]_{\mathrm{nr}} P_1{}^+(\sigma_1) + \left[\frac{P_2{}^+}{P_2{}^-}\right]_{\mathrm{nr}} P_2{}^-(\sigma_1) \tag{37}$$

$$P_1{}^-(P_1{}^+) = \left[\frac{P_1{}^-}{\sigma_1}\right]_{\mathrm{nr}} \sigma_1(P_1{}^+) + \left[\frac{P_1{}^-}{P_1{}^+}\right]_{\mathrm{nr}} P_1{}^+(P_1{}^+) + \left[\frac{P_1{}^-}{P_2{}^-}\right]_{\mathrm{nr}} P_2{}^-(P_1{}^+) \tag{38}$$

$$P_2{}^+(P_1{}^+) = \left[\frac{P_2{}^+}{\sigma_1}\right]_{\mathrm{nr}} \sigma_1(P_1{}^+) + \left[\frac{P_2{}^+}{P_1{}^+}\right]_{\mathrm{nr}} P_1{}^+(P_1{}^+) + \left[\frac{P_2{}^+}{P_2{}^-}\right]_{\mathrm{nr}} P_2{}^-(P_1{}^+) \tag{39}$$

$$P_1{}^-(P_2{}^-) = \left[\frac{P_1{}^-}{\sigma_1}\right]_{\mathrm{nr}} \sigma_1(P_2{}^-) + \left[\frac{P_1{}^-}{P_1{}^+}\right]_{\mathrm{nr}} P_1{}^+(P_2{}^-) + \left[\frac{P_1{}^-}{P_2{}^-}\right]_{\mathrm{nr}} P_2{}^-(P_2{}^-) \tag{40}$$

$$P_2{}^+(P_2{}^-) = \left[\frac{P_2{}^+}{\sigma_1}\right]_{\mathrm{nr}} \sigma_1(P_2{}^-) + \left[\frac{P_2{}^+}{P_1{}^+}\right]_{\mathrm{nr}} P_1{}^+(P_2{}^-) + \left[\frac{P_2{}^+}{P_2{}^-}\right]_{\mathrm{nr}} P_2{}^-(P_2{}^-) \tag{41}$$

where the forcing type is given in parenthesis, and the subscript nr indicates that the transfer functions are non-reflective.

### *3.3. Results*

Entropy noise levels and acoustic wave propagation in the DISCERN nozzle resulting from both CHEOPS-Nozzle and CAA are discussed in this section. The transfer functions resulting from the acceleration of an entropy wave through the domain are given in Fig. 5. The entropy noise computed by CAA is maximal around 300 Hz and becomes relatively low in the upper end of the frequency range. Also note the transmitted acoustic wave $P_2^+$ exhibits noise levels about ten times greater than its regressive counterpart $P_1^-$. Figure 5 also shows results from two analytical models from the literature - Marble and Candel's model for the compact case [13] and a one-dimensional model [17, 39] - as well as those given by CHEOPS-Nozzle. The compact model and CAA seem to be in agreement, but the compact solution is only valid for very low frequencies while the amplitude of the transfer functions quickly evolves. The one-dimensional model captures this evolution but in a very limited low frequency range, as amplitudes are grossly overestimated for both transfer functions from about 200 Hz. The 2D-model CHEOPS-Nozzle allows to overcome this, since its estimated noise

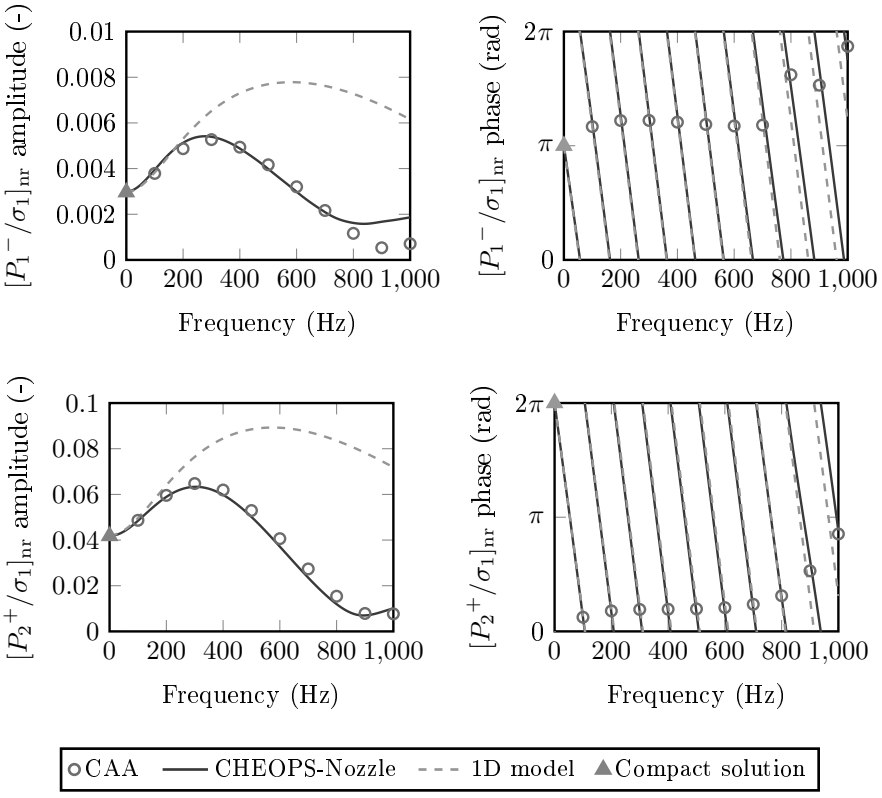


Figure 5: Amplitude and phase of the transfer functions resulting from entropic forcing $[P_1^-/\sigma_1]_{\mathrm{nr}}$ (top) and $[P_2^+/\sigma_1]_{\mathrm{nr}}$ (bottom) computed using CAA, CHEOPS-Nozzle, a one-dimensional model [17, 39] and Marble and Candel's compact solution [13].

levels are in good accordance with CAA. The amplitude of $[P_1^-/\sigma_1]_{\mathrm{nr}}$ is nevertheless overestimated by the model at high frequency, above about 800 Hz, which could be caused by the stronger assumptions taken by CHEOPS-Nozzle compared to CAA: one-dimensional acoustic waves and negligible vorticity. The phase of the transfer functions has a large slope due to a low convection speed, but it is shown between $[0, 2\pi]$ in Fig. 5 to allow comparison of the different methods. All phases agree in the compact limit but there are small errors in 1D at high frequency compared to the two-dimensional approaches. These latter methods are in good agreement, showing convection and propagation are correctly accounted for by CHEOPS-Nozzle. Overall, one can consider CHEOPS-Nozzle gives a good estimate of the entropy noise generated in the DISCERN nozzle.

This comparison highlights the significance of radial effects on entropy noise, as taken into account by CHEOPS-Nozzle. They can be due to the two-

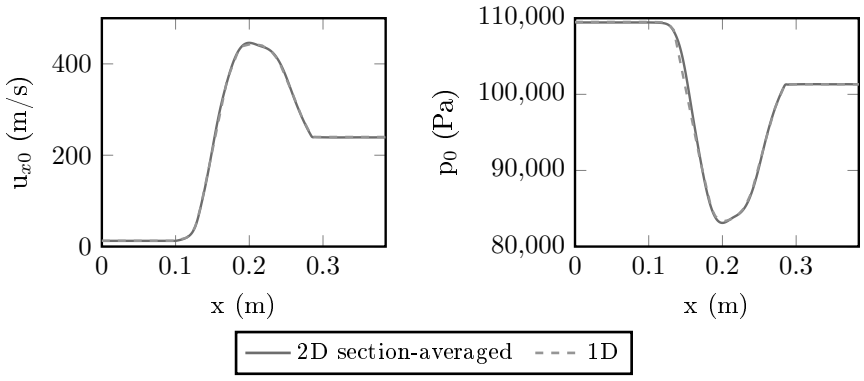


Figure 6: Mean axial velocity (left) and pressure (right) profiles used by the 2D model CHEOPS-Nozzle after sectional averaging and by a 1D model [17, 39].

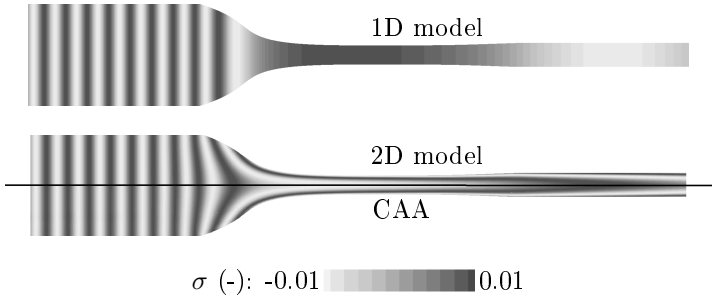


Figure 7: Contour of the normalised entropy fluctuations $\sigma$ inside the DISCERN nozzle in 1D (top) and obtained analytically and numerically in 2D (bottom) for harmonic forcing at 1000 Hz.

dimensionality of either the mean flow or the entropy wave. Figure 6 represents one-dimensional mean flow quantities along the nozzle axis, as well as two-dimensional values averaged over each section in the same way as for CHEOPS-Nozzle. There are only slight differences between the 1D and 2D averaged values, so that two-dimensional mean flow effects do not appear to be responsible for the lower entropy noise levels. Figure 7 shows the normalised entropy fluctuation contours used by the 1D and 2D models, as well as those obtained through CAA. First note the contours resulting from the numerical and analytical approaches in 2D are in agreement, verifying entropy wave dispersion is correctly computed by CHEOPS-Nozzle. Secondly, unlike the mean flow quantities in Fig. 6, the normalised entropy fluctuation contours used by the 1D and 2D models differ significantly. It seems the two-dimensional nature of this entropy wave leads to source decorrelation at sufficiently high frequencies as it is accelerated through the nozzle, which explains the reduction of entropy

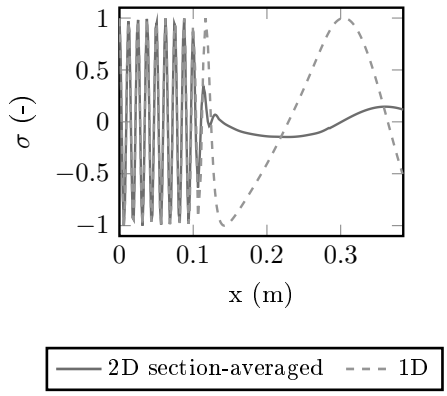


Figure 8: Normalised entropy fluctuations used by the 2D model CHEOPS-Nozzle after sectional averaging and by a 1D model [17, 39].

noise in two dimensions observed in Fig. 5. The effect of this source decorelation is also illustrated by Fig. 8. In the same way as Fig. 6 for mean quantities, it represents the axial evolution of normalised entropy perturbations in a 1D nozzle and sectionally averaged in 2D. It shows radial variations of the flow lead to a significant reduction in the amplitude of entropy fluctuations from the convergent part of the nozzle, corresponding to a weaker source strength.

Like with entropy forcing, transfer functions corresponding to upstream and downstream acoustic excitation are represented in Fig. 9 and Fig. 10 respectively. Results from CHEOPS-Nozzle are in good agreement with both CAA and Marble and Candel's compact solution [13], which confirms the good scattering of acoustic waves by the model. Data from the one-dimensional model also agrees with these two-dimensional results, confirming the validity of the one-dimensional acoustics assumption made within CHEOPS-Nozzle.

## 4. Conclusions

The semi-analytical model CHEOPS-Nozzle for entropy noise in subsonic nozzle flow has been presented. It is based on the Euler equations and it takes the 2D-axisymmetric nature of the flow into account. It was validated with a Euler mean flow field by comparison with a reference case built using a novel CAA approach. This method was chosen because it is also based on the Euler equations, making it analogous to the framework of the model with two notable differences: acoustics are not considered one-dimensional and vorticity is not neglected by the CAA method. The first of these assumptions was verified numerically. The concordance of the noise levels given by the model and CAA seems to indicate the negligible vorticity assumption is also valid. Good agreement was found for the three possible excitation types: entropic, upstream acoustic and downstream acoustic. In addition, these results match Marble and

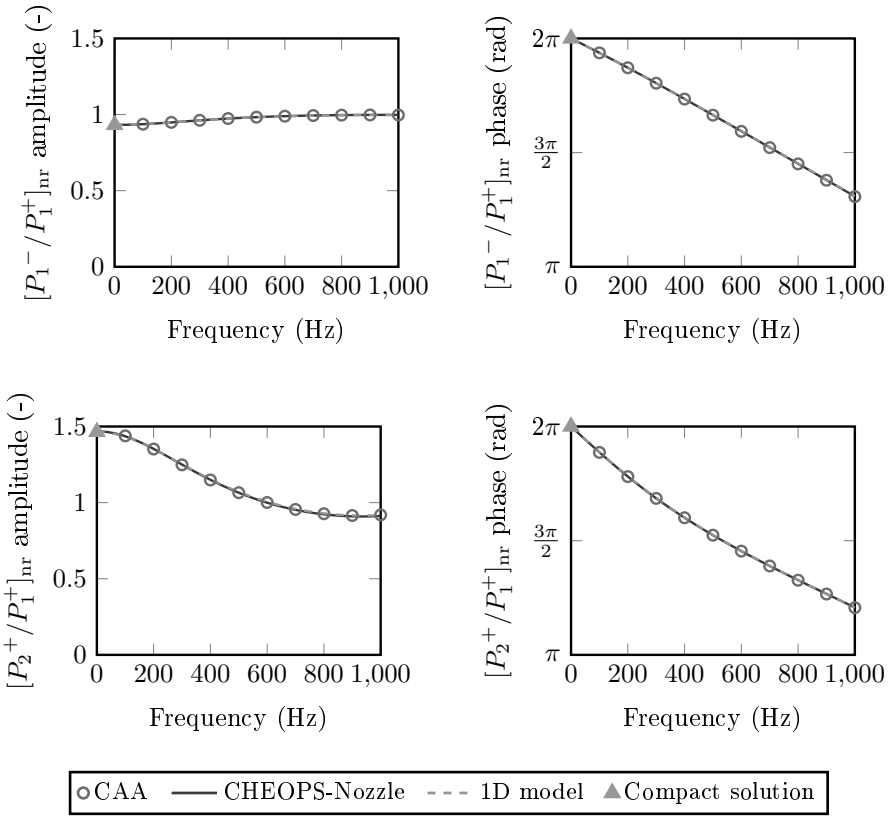


Figure 9: Amplitude and phase of the transfer functions resulting from upstream acoustic forcing $[P_1{}^-/P_1^+]_{\mathrm{nr}}$ (top) and $[P_2{}^+/P_1^+]_{\mathrm{nr}}$ (bottom) computed using CAA, CHEOPS-Nozzle, a 1D model [17, 39] and Marble and Candel's compact solution [13].

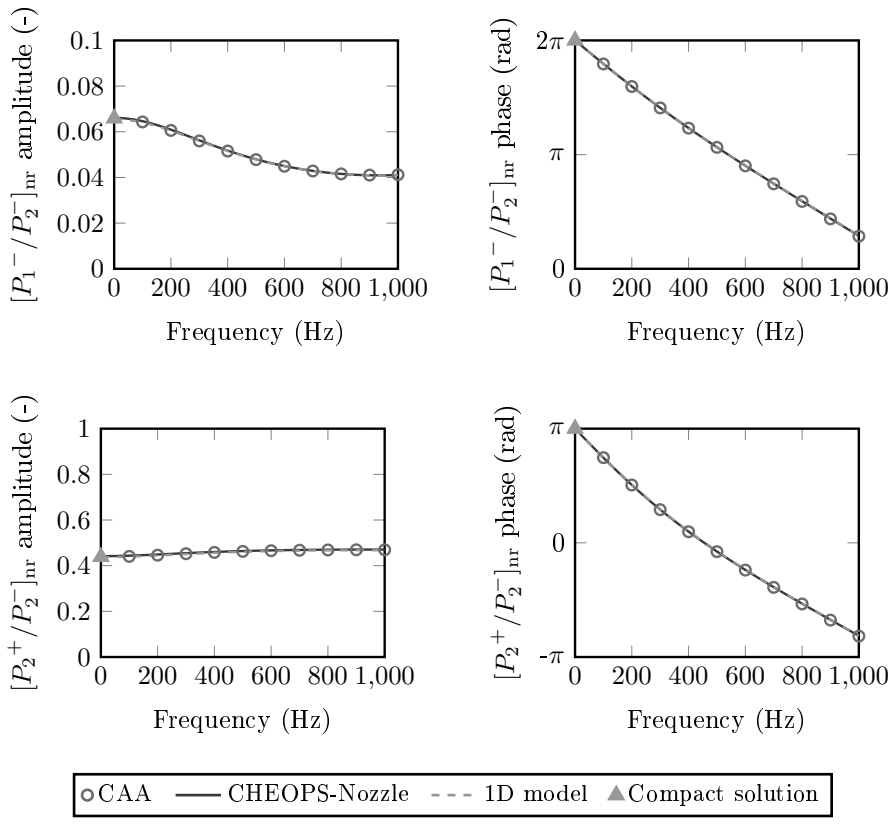


Figure 10: Amplitude and phase of the transfer functions resulting from downstream acoustic forcing $[P_1{}^-/P_2^-]_{\mathrm{nr}}$ (top) and $[P_2{}^+/P_2^-]_{\mathrm{nr}}$ (bottom) computed using CAA, CHEOPS-Nozzle, a 1D model [17, 39] and Marble and Candel's compact solution [13].

Candel's compact solution [13]. This study allowed to highlight the significance of two-dimensional effects on entropy noise, which seem to be due to the deformation of the entropy wave and the subsequent decorrelation of acoustic sources throughout the nozzle.

## References


[1] A. P. Dowling, Y. Mahmoudi, Combustion Noise, Proceedings of the Combustion Noise Institute 35 (1) (2015) 65–100.

[2] M. Ihme, Combustion and Engine-Core Noise, Annual Review of Fluid Mechanics 49 (2017) 277–310.

[3] T. Livebardon, S. Moreau, L. G. T. Poinsot, E. B. Combustion, Flame, Combining LES of Combustion Chamber and an Actuator Disk Theory to Predict Combustion Noise in a Helicopter Engine, Combustion and Flame 165 (2016) 272–287.

[4] M. Férand, T. Livebardon, S. Moreau, M. Sanjosé, Numerical Prediction of Far-Field Combustion Noise from Aeronautical Engines, Acoustics 1 (1) (2019) 174–198.

[5] W. Polifke, C. O. Paschereit, D. Klaus, Constructive and Destructive Interference of Acoustic and Entropy Waves in a Premixed Combustor with a Choked Exit, International Journal of Acoustics and Vibrations 6 (3) (2001) 135–146.

[6] C. K. W. Tam, F. Bake, L. S. Hultgren, T. Poinsot, Aircraft Noise Generation and Assessment, CEAS Aeronautical Journal 10 (1) (2019) 101–122.

[7] L. Magri, J. O'Brien, M. Ihme, Compositional Inhomogeneities as a Source of Indirect Combustion Noise, Journal of Fluid Mechanics 799 (7) (2016) R4.

[8] N. Kings, Indirect Combustion Noise: Experimental Investigation of the Vortex Sound Generation in Nozzle Flows, Ph.D. thesis, Technischen Universität Berlin (2014).

[9] M. Howe, Indirect Combustion Noise, Journal of Fluid Mechanics 659 (2010) 267–288.

[10] E. Rolland, F. De Domenico, S. Hochgreb, Direct and Indirect Noise Generated by Entropic and Compositional Inhomogeneities, Journal of Engineering for Gas Turbines and Power 140 (8) (2018) 082604.

[11] B. Chu, L. S. G. Kovásznay, Non-linear Interactions in a Viscous Heat-conducting Compressible Gas, Journal of Fluid Mechanics 3 (5) (1958) 494–514.

[12] C. K. W. Tam, S. A. Parrish, The Physical Processes of Indirect Combustion Noise Generation, International Journal of Aeroacoustics 17 (2) (2018) 22–35.

[13] F. E. Marble, S. M. Candel, Acoustic Disturbance from Gas Nonuniformities Convected Through a Nozzle, Journal of Sound and Vibration 55 (2) (1977) 225–243.

[14] N. A. Cumpsty, F. E. Marble, The Interaction of Entropy Fluctuations with Turbine Blade Rows; A Mechanism of Turbojet Engine Noise, Proceedings of the Royal Society of London A 357 (1977) 323–344.

[15] J. Li, A. S. Morgans, Time Domain Simulations of Non-linear Thermoacoustic Stability of a Model Combustor, Journal of Sound and Vibration 346 (2015) 345–360.

[16] A. S. Morgans, C. S. Goh, J. A. Dahan, The Dissipation and Shear Dispersion of Entropy Waves in Combustor Thermodynamics, Journal of Fluid Mechanics 733 (R2).

[17] M. Huet, F. Vuillot, N. Bertier, M. Mazur, N. Kings, W. Tao, P. Scouflaire, F. Richecoeur, S. Ducruix, C. Lapeyre, T. Poinsot, Recent Improvements in Combustion Noise Investigation: from the Combustion Chamber to Nozzle Flow, Aerospace Lab 11 (10).

[18] P. Gaetani, G. Persico, A. Spinelli, Entropy Wave Generator for Indirect Combustion Noise Experiments in a High-Pressure Turbine, in: 11th European Turbomachinery Conference, no. ETC2015-025, Madrid, Spain, 2015.

[19] M. Férand, G. Daviller, S. Moreau, C. Sensiau, T. Poinsot, Using LES for Combustion Noise Propagation to the Far-field by Considering the Jet Flow of a Dual-stream Nozzle, in: AIAA/CEAS Aeroacoustics Conference, AIAA AVIATION Forum , no. AIAA 2018–3282, Atlanta, USA, 2018.

[20] N. Kings, W. Tao, P. Scouflaire, F. Richecoeur, S. Ducruix, Experimental and Numerical Investigation of Direct and Indirect Combustion Noise in a Lean Premixed Laboratory Swirled Combustor, in: ASME Turbo Expo, no. GT2016–57848 in 4B, Seoul, South Korea, 2016.

[21] F. Bake, C. Richter, B. Mühlbauer, N. Kings, I. Röhle, F. Thiele, B. Noll, The Entropy Wave Generator (EWG): a Refence Case on Entropy Noise, Journal of Sound and Vibration 326 (3-5) (2009) 574–598.

[22] W. C. Ullrich, J. Gikadi, C. Jörg, T. Sattelmayer, Acoustic-entropy Coupling Behavior and Acoustic Scattering Properties of a Laval Nozzle, in: 20th AIAA/CEAS Aeroacoustics Conference, AIAA Aviation, no. AIAA 2014-3193, Atlanta, USA, 2014.

[23] S. Moreau, C. Becerril Aguirre, L. Gicquel, Large-eddy-simulation Prediction of Indirect Combustion Noise in the Entropy Wave Generator Experiment, International Journal of Spray and Combustion Dynamics 10 (2) (2018) 154–168.

[24] M. Leyko, S. Moreau, F. Nicoud, T. Poinsot, Numerical and Analytical Modelling of Entropy Noise in a Supersonic Nozzle with a Shock, Journal of Sound and Vibration 330 (16) (2011) 3944–3958.

[25] C. Becerril Aguirre, S. Moreau, M. Bauerheim, L. Gicquel, T. Poinsot, Numerical Investigation of Combustion Noise: The Entropy Wave Generator, in: 22nd AIAA/CEAS Aeroacoustics Conference, Aeroacoustics Conferences , no. AIAA 2016-2830, Lyon, France, 2016.

[26] J. M. Lourier, A. Huber, B. Noll, M. Aigner, Numerical Analysis of Indirect Combustion Noise Generation Within a Subsonic Nozzle, AIAA Journal 52 (10) (2014) 2114–2126.

[27] C. Richter, F. Thiele, Computation of Indirect Combustion Noise by a CAA-method, in: 14th International Congress on Sound and Vibration, Cairns, Australia, 2007.

[28] K. Knobloch, T. Werner, F. Bake, Entropy Noise Generation and Reduction in a Heated Nozzle Flow, in: 21st AIAA/CEAS Aeroacoustics Conference, AIAA AVIATION Forum , no. AIAA 2015–2818, Dallas, USA, 2015.

[29] K. Knobloch, T. Werner, F. Bake, Noise Generation in Hot Nozzle Flow, in: ASME Turbo Expo, no. GT2015-43702, Montreal, Canada, 2015.

[30] F. De Domenico, E. O. Rolland, S. Hochgreb, Detection of Direct and Indirect Noise Generated by Synthetic Hot Spots in a Duct, Journal of Sound and Vibration 394 (2017) 220–236.

[31] J. H. Miles, Separating Direct and Indirect Engine Combustion Noise using the Correlation Function, Journal of Propulsion and Power 26 (5) (2010) 1144–1152.

[32] B. Pardowitz, U. Tapken, K. Knobloch, F. Bake, E. Bouty, I. Davis, G. Bennett, Core Noise Identification of Broadband Noise Sources of a Turbo-shaft Engine, in: 20th AIAA/CEAS Aeroacoustics Conference, AIAA Aviation, no. AIAA 2014-3321, Atlanta, USA, 2014.

[33] B. Schuster, G. Gordon, L. S. Hultgren, Dynamic Temperature and Pressure Measurements in the Core of a Propulsion Engine, in: 21st AIAA/CEAS Aeroacoustic Conference, no. AIAA 2015-2819, Dallas, USA, 2015.

[34] C. K. W. Tam, S. A. Parrish, J. Xu, B. Schuster, Indirect Combustion Noise of Auxiliary Power Units, Journal of Sound and Vibration 332 (2013) 4004–4020.

[35] C. K. W. Tam, S. A. Parrish, Noise of High-performance Aircraft at Afterburner, Journal of Sound and Vibration 352 (2015) 103–128.

[36] M. Huet, A. Giauque, A Nonlinear Model for Indirect Combustion Noise Through a Compact Nozzle, Journal of Fluid Mechanics 733 (2013a) 268–301.

[37] S. R. Stow, A. P. Dowling, T. P. Hynes, Reflection of Circumferential Modes in a Choked Nozzle, Journal of Fluid Mechanics 467 (2002) 215–239.

[38] W. Moase, M. J. Brear, C. Manzie, The Forced Response of Choked Nozzles and Supersonic Diffusers, Journal of Fluid Mechanics 585 (2007) 281–304.

[39] A. Giauque, M. Huet, F. Cléro, Analytical Analysis of Indirect Combustion Noise in Subcritical Nozzles, Journal of Engineering for Gas Turbines and Power 134 (11) (2012) 111202.

[40] I. Durán, S. Moreau, Solution of the Quasi-one-dimensional Linearized Euler Equations Using Flow Invariants and the Magnus Expansion, Journal of Fluid Mechanics 723 (2013) 190–231.

[41] C. S. Goh, A. S. Morgans, Phase Prediction of the Response of Choked Nozzles to Entropy and Acoustic Disturbances, Journal of Sound and Vibration 330 (21) (2011) 5184–5198.

[42] E. Rolland, F. De Domenico, S. Hochgreb, Theory and Application of Reverberated Direct and Indirect Noise, Journal of Fluid Mechanics 819 (2017) 435–464.

[43] F. De Domenico, E. Rolland, S. Hochgreb, A Generalised Model for Acoustic and Entropic Transfer Function of Nozzles with Losses, Journal of Sound and Vibration 440 (2019) 212–230.

[44] I. Durán, A. S. Morgans, On the Reflection and Transmission of Circumferential Waves Through Nozzles, Journal of Fluid Mechanics 773 (2015) 137–153.

[45] T. Sattelmayer, Influence of the Combustor Aerodynamics on Combustion Instabilities from Equivalence Ratio Fluctuations, Journal of Engineering for Gas Turbines and Power 125 (2003) 11–19.

[46] A. Giusti, N. A. Worth, E. Mastorakos, A. P. Dowling, Experimental and Numerical Investigation into the Propagation of Entropy Waves, AIAA Journal 55 (2) (2016) 446–458.

[47] Y. Xia, I. Durán, A. Morgans, X. Han, Dispersion of Entropy Perturbations Transporting through an Industrial Gas Turbine Combustor, Flow Turbulence and Combustion 100 (2) (2018) 481–502.

[48] A. Fattahi, S. M. Hosseinalipour, N. Karimi, On the Dissipation and Dispersion of Entropy Waves in Heat Transferring Channel Flows, Physics of Fluids 29 (8).

[49] Y. Mahmoudi, A. Giusti, E. Mastorakos, A. P. Dowling, Low-Order Modeling of Combustion Noise in an Aero-Engine: The Effect of Entropy Dispersion, Journal of Engineering for Gas Turbines and Power 140 (1) (2018) 011502.

[50] C. C. Becerril Aguirre, S. Moreau, L. Y. M. Gicquel, Study of Combustion Noise Generation in a Realistic Turbine Stage Configuration, in: ASME Turbo Expo, no. GT2018–75062 in 2B, Oslo, Norway, 2018.

[51] C. Becerril Aguirre, Simulation of noise emitted by a reactive flow, Ph.D. thesis, INP Toulouse (2017).

[52] M. Leyko, S. Moreau, F. Nicoud, T. Poinsot, Simulation and Modelling of the Waves Transmission and Generation in a Stator Blade Row in a Combustion-Noise Framework, Journal of Sound and Vibration 333 (23) (2014) 6090–6106.

[53] M. Bauerheim, I. Durán, T. Livebardon, G. Wang, S. Moreau, T. Poinsot, Transmission and Reflection of Acoustic and Entropy Waves through a Stator-rotor Stage, Journal of Sound and Vibration 374 (2016) 260–278.

[54] J. Zheng, M. Huet, A. Giauque, F. Cléro, S. Ducruix, A 2D-axisymmetric Analytical Model for the Estimation of Indirect Combustion Noise in Nozzle Flows, in: 21st AIAA/CEAS Aeroacoustics Conference, AIAA Aviation, no. AIAA 2015-2974, Dallas, USA, 2015.

[55] J. Zheng, Analytical and Numerical Study of the Indirect Combustion Noise Generated by Entropy Disturbances in Nozzle Flows, PhD Thesis, Université Paris Saclay (2016).

[56] A. Giauque, M. Huet, F. Cléro, S. Ducruix, F. Richecoeur, Thermoacoustic Shape Optimization of a Subsonic Nozzle, Journal of Engineering for Gas Turbines and Power 135 (10) (2013) 102601.

[57] S. Redonnet, E. Manoha, P. Sagaut, Numerical Simulations of Propagation of Small Perturbations Interacting with Flows and Solid Bodies, in: 7th AIAA/CEAS Aeroacoustics Conference, Aeroacoustics Conferences , no. AIAA 2001-0222, Maastricht, Netherlands, 2001.

[58] S. Redonnet, Numerical Study of Acoustic Installation Effects with a Computational Aeroacoustics Method, AIAA Journal 48 (5) (2010) 929–937.

[59] C. K. W. Tam, Z. Dong, Radiation and Outflow Boundary Conditions for Direct Computation of Acoustic and Flow Disturbances in a Nonuniform Mean Flow, Journal of Computational Acoustics 4 (2) (1996) 175–201.

[60] C. K. W. Tam, J. Webb, Dispersion-Relation-Preserving Finite Difference Schemes for Computational Acoustics, Journal of Computational Physics 107 (2) (1993) 262–281.